Deep Mining 2024 – P Andrieux & D Cumming-Potvin (eds)

doi:10.36487/ACG_repo/2465_41

Excess shear stress analysis of complex geological structures in underground mines

Gerhard F Hofmann [a,*]

[a] *AngloGold Ashanti, South Africa*

Abstract

Shear deformation on weak geological structures, such as shear zones, faults or orebody contacts, can pose a significant seismic hazard in underground mines. The mine geological model can be complex, and when the whole underground mine is considered by elastic numerical modelling, the dataset can be large and challenging to manage using commercially available modelling software. A procedure has been developed to use the triangulation defining the geometrical models of structures directly, not requiring any surface fitting or simplification. The polygon orientations and stress tensors from boundary element numerical modelling, are used to calculate the normal and shear stress components at the centroid of each polygon, from which excess shear stress is derived as a failure criterion for structure-related seismic hazard.

The proposed procedure enables visualisation of modelled excess shear stress for the full geological model, highlighting areas of potential co-seismic shear deformation along structures. It is also useful to quantify and visualise the modelled seismic hazard relative to mine tunnels, since this is where mine workers are exposed. A statistical approach is used to derive consistent, quantified overstressing values accounting for possible unrealistic results from elastic modelling.

The methodology is described in a case study for a sublevel stoping mine, currently at a depth of 1,000 m. The geological model is large and complex, and it is a challenge to analyse and represent structure-related seismic hazard. The historical conditions were used to derive and verify modelling criteria, which were then used to simulate expected conditions to 2,000 m below surface. The methodology was used to assess the seismic hazard by identifying the potential for large events and tunnels vulnerable to damaging ground motions.

Keywords: *underground mine seismic hazard, numerical stress modelling, excess shear stress, geological structure model*

1 Introduction

In some underground mining environments, for example the South African deep level tabular mines, geological faults pose a seismic hazard, potentially yielding fault slip events under mining-induced stress changes. These faults are typically sub-planar features, and from a modelling point of view it is easy to build a surface geometrical model of the structure. Such structures can be built by regular-shaped triangular or rectangular shapes along which elastic overstressing or non-linear displacement can be modelled using boundary element numerical modelling code (Hofmann et al. 2013). This would also be the case for joints or shear zones which are generally sub-planar. However, in other mining environments with foliation, folding and various lithologies, such geological models can be complex and the number of elements required to define the geometry can be excessive.

Geological structure models are usually defined as triangular elements, and for complex geometries, the triangle sizes will be smaller to capture detail. Elastic stress boundary element numerical modelling software, such as *Map3D* (Wiles 2024), has the capability to simulate non-linear ride on displacement-discontinuity (DD)

* Corresponding author. Email address: ghofmann@anglogoldashanti.com

elements, however, subject to the size and complexity of geological structures it may be the case that the matrix solution does not converge.

To assess seismic hazard associated with complex structures (e.g. folded contacts), it is therefore not feasible to build them as DD elements and import them into the boundary element model. Even if a small model is set up, it is likely that the model would not converge, and it will be virtually impossible to derive results on mine-scale.

The so-called Triangulation-ESS (excess shear stress) methodology is proposed here to assess seismic hazard for complex geological models, which can be large and include multiple structures. This would typically be the case for weak lithology contacts, and depending on their orientation in the stress field, may pose a significant seismic hazard.

2 The Triangulation-ESS methodology for geological structures

The methodology comprises of firstly importing the triangulation model as is, but discarding elements based on undesirable shapes and sizes. All triangulation elements are tested in terms of validity (some erroneous elements may for example repeat vertices), area, and aspect ratio, and eliminating elements which would not contribute constructively to stress analysis. For example, elements smaller than 0.1 m^2 area, and aspect ratio greater than 100 are discarded. Otherwise, for all valid elements, it is possible to extract the centroid coordinates, and the dip and dip direction which defines its spatial orientation. This is the important aspect, since the orientation of a plane in the stress field determines the shear stress and normal stress, as required for Mohr–Coulomb strength.

The next step is to apply a software option (for example in *Map3D*) to provide coordinates in an external text file and calculate any stress-components, strain-components or displacement-components. In the approach described here, the six Cartesian stress components are written out as a text file for all the structure triangulation centroid coordinates for the selected points.

The dip and dip direction are required to do the standard stress transformation to get normal stress and shear stress for each element from which ESS can be calculated as per the Mohr–Coulomb shear strength failure criterion (Ryder 1988):

$$\mathrm{ESS} = \tau - (\mathrm{C} + \sigma_N \tan(\varphi_f)) \quad (1)$$

where:

- τ and σ_N = the modelled shear stresses and normal stresses respectively on a particular plane orientation (defined by dip and dip direction), for a geological discontinuity.
- C = the cohesion (internal strength) on the plane.
- $\tan(\varphi_f)$ = the friction coefficient which scales the increase in shear strength by normal stress clamping, usually given by the friction angle φ_f.

As part of the procedure, it is required to quantify ESS statistically, and therefore it is beneficial to set up triangulation elements of approximately similar size. As mentioned, element area sizes of the geological structure models can vary significantly, subject to the complexity of the surface. Therefore, before calculation of results, elements are subdivided into approximately equal areas. Although this increases the number of points, it simply means longer computer runtimes but would not affect the model convergence.

The above description is now illustrated for a real case of a banded iron formation (BIF) lithology, where the contacts can be weak and known to give ground control problems as well as yield seismic events.

2.1 ESS modelling of a complex lithological contact

A perspective north-westerly section view of a complex BIF lithology geometrical model between mining levels 19 and 21 is shown in Figure 1. This is from a gold mine at around 1,000 m depth below surface, with mineralisation of the BIF contacts being mined as the main orebody. The triangulation is not visible in the figure, and the elements can be very small and typically include 'bad' shapes for boundary element modelling, in particular poor aspect ratios and sharp angles. In this case the number of elements is approximately 300,000. Element area sizes vary between 0.001–1,000 m^2, and aspect ratios (defined as maximum divided by minimum side length) of more than 1,000 are found. Hence, these triangulation shapes are not suitable for conventional boundary element modelling by importing them as boundary elements and solving for shear stresses and normal stresses, whether to consider elastic ESS or non-linear ride.

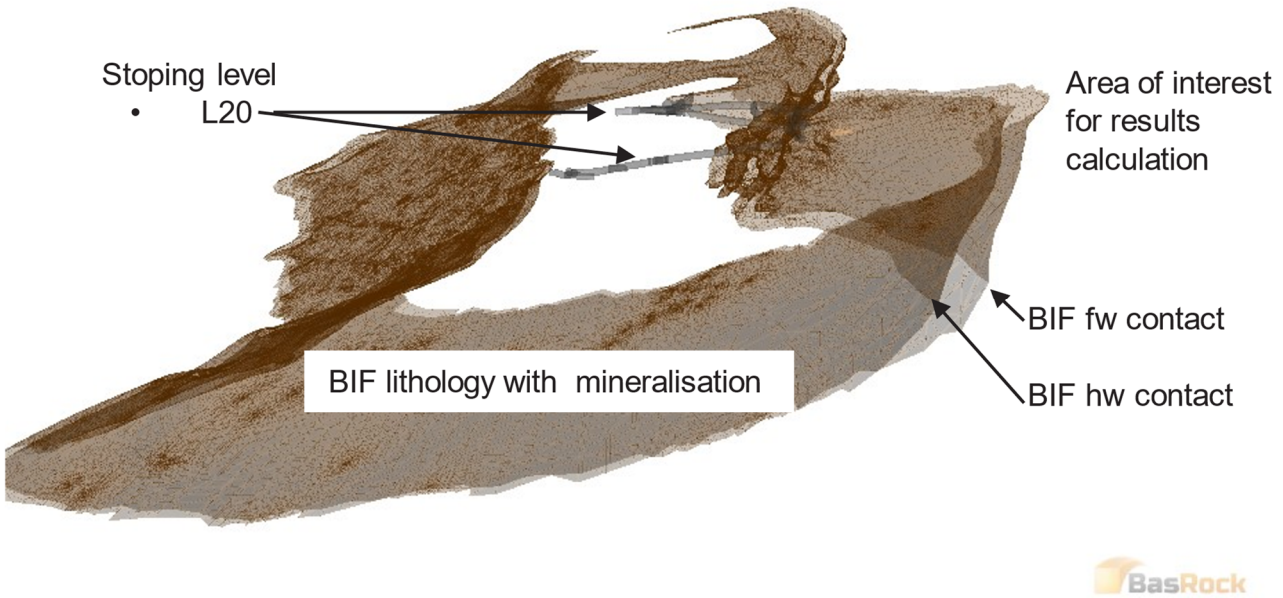

Figure 1 Section perspective north-westerly view, updip along the banded iron formation lithology, with the structure shown around mining levels 19 to 21. The triangulation model of the banded iron formation contacts was incorporated for excess shear stress analysis. Although only this one lithology is considered here, it can be deemed as a complex structure that cannot be modelled as displacement-discontinuity elements in boundary element code. Note: fw = footwall, hw = hanging wall

Figure 2 is a close-up view of a selected area on the structure (indicated in Figure 1 as the area of interest), and only the BIF footwall contact. The filtering procedure discarded elements smaller than 0.1 m^2 area, and the larger elements were subdivided to be smaller than 20 m^2. Furthermore, a maximum aspect ratio of 100 was allowed. This caused the number of elements to change from to 17,741 to 10,219, therefore so many points for stress calculation following convergence of a model step. The number of points naturally determine the calculation time, which in this case was less than 2 minutes in *Map3D*. As a reference, the same Triangulation-ESS models for other sites comprised of 2.6 million points, which could also be managed by *Map3D* and the methodology proposed here.

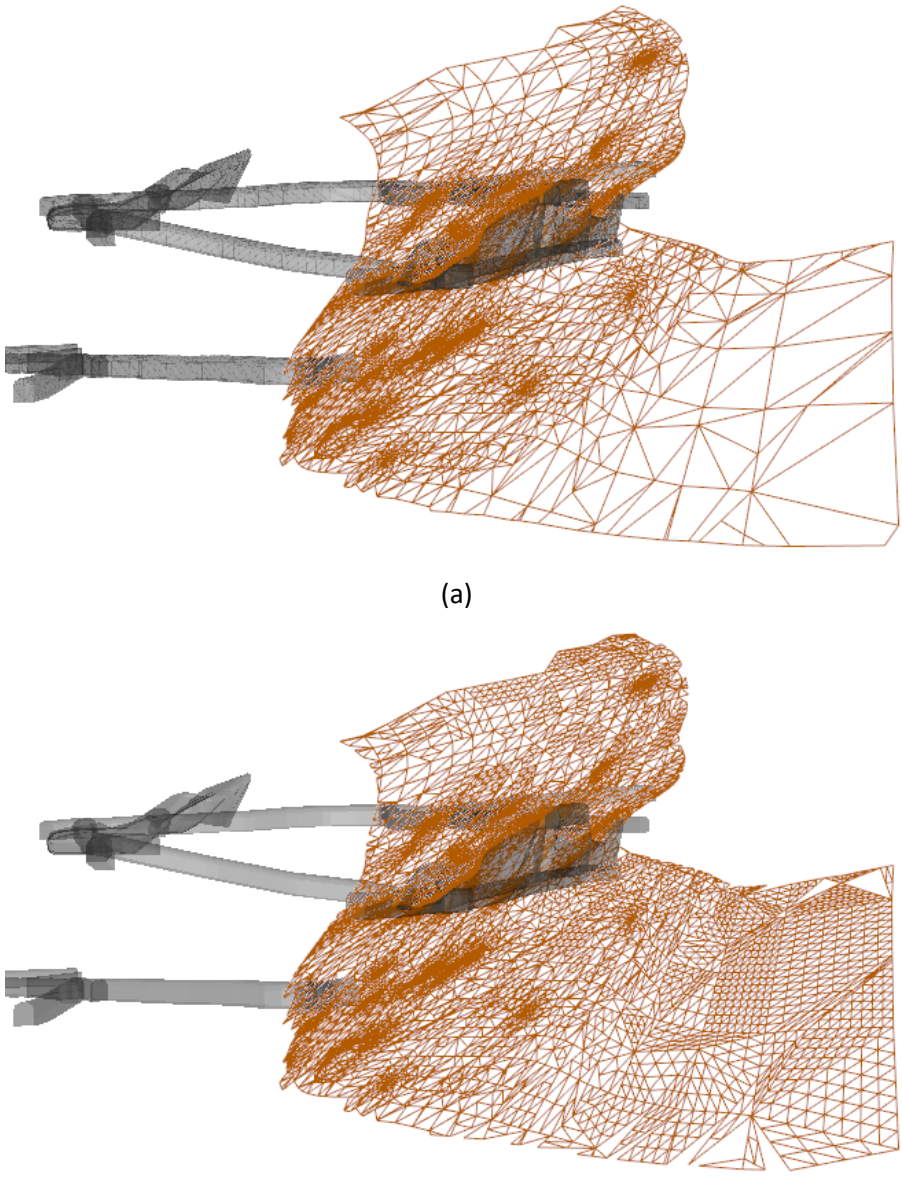

(a)

(b)

Figure 2 One area of the banded iron formation lithology is shown to illustrate (a) the triangulation used as input geological model and (b) the processing thereof to be more suitable for modelling of the surface shear stress and normal stress

After importing and filtering, the next step is to calculate ESS from the Cartesian stress components and element dip and dip direction, which can be done outside of *Map3D* using Python code (Python 2024) written for this purpose. Standard 3D stress transformations are applied to derive normal stress and shear stress on the element plane orientation. The resulting picture of structure ESS is shown in Figure 3. The outlined area of increased ESS is below the stoping around the northern part of the main orebody, and the interpretation is that the BIF footwall contact shows the potential for shear slip subject to the structure orientation in the mining-induced stress field. Such a 'lobe' of ESS indicates the potential for a seismic event, caused mainly by the unclamping of a weak geological feature, although loaded in shear already by the pre-mining stress field.

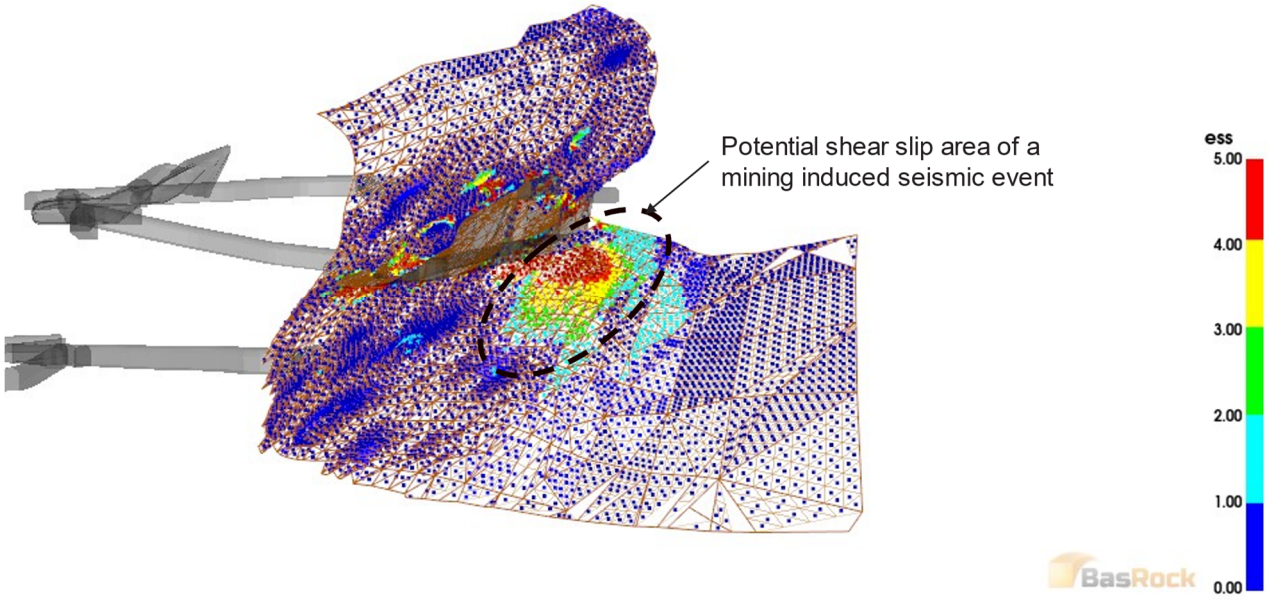

Figure 3 Modelled excess shear stress (ESS) for the banded iron formation footwall contact is shown by the colour-contoured dots at the element centroids. The outlined area is interpreted as a 'lobe' of ESS indicating the potential for a shear slip seismic event. This positive ESS area is mainly due to unclamping by the stoping in the stress field, even though the stoping is limited

2.2 Statistical quantification of structure ESS

It is now proposed to quantify the level of overstressing based on a statistical probability of failure approach, instead of simply the average.

The distribution of ESS for the dataset is shown in Figure 4. This shows firstly a histogram bar chart of ESS from which the normalised cumulative distribution can be derived, shown by the dots and referred to as the 'ecdf' – **e**mpirical **c**umulative **d**istribution **f**unction (Ford 2020). This gives the probability for a grid point stress value to exceed a particular threshold. A univariate spline is fitted through the ecdf to allow calculation of the probability for exceedance at any stress value. The gradient of the ecdf is the probability distribution, based on the actual modelling data and not, for example, a normal (Gaussian) distribution. The distribution is considered up to the point where the ecdf is reliable, therefore outliers can be discarded and small data sets can be handled.

The above procedure is also implemented by Python coding (Python 2024) where a number of functions from the numerical module is used to set up the cumulative histogram, fit and smooth the spline function, and generate the graphs and more.

In the case of ESS, which is an excess stress parameter, a criterion of 0 MPa is applicable to quantify the probability for positive values for the dataset, which in this case is interpreted as the probability for shear slip. It is referred to as the Probability of Failure (PoF) here and quantifies the potential for positive ESS which is the area under the probability distribution. For the example in Figure 3, based on the ESS distribution in Figure 4, the PoF is derived as 0.234. In Section 3 it will be discussed how a damaging seismic event, evidently associated with the BIF footwall contact, is used as calibration of the geology structure-related seismic hazard to derive a PoF which can be used to assess the seismic hazard for planned mining.

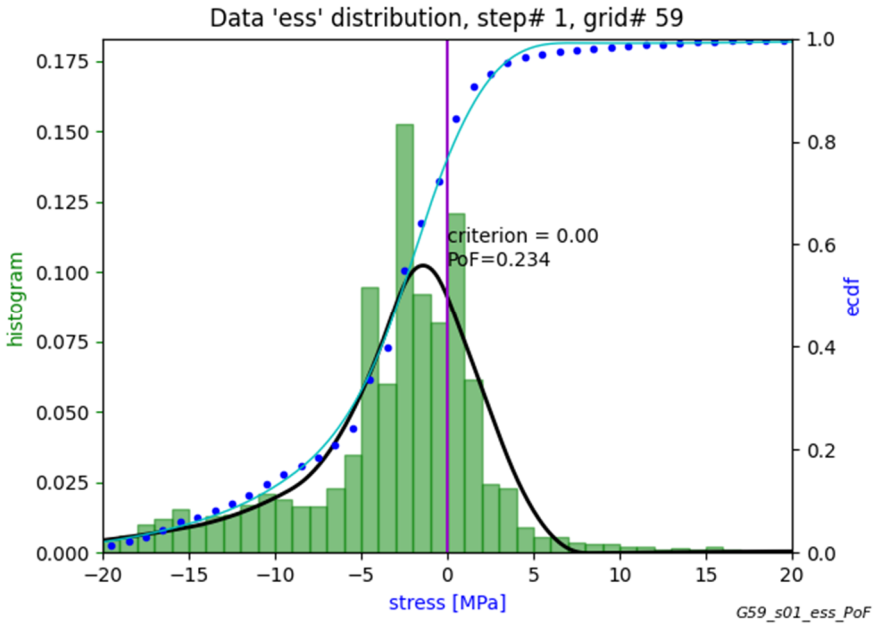

Figure 4 Proposed statistical approach to quantify the level of overstressing, in this case excess shear stress along the banded iron formation footwall contact shown in Figure 3. The empirical cumulative distribution function (ecdf) is derived by fitting a spline through the cumulative histogram. The gradient of the ecdf is then the empirical probability distribution (black line), from which the area under the normalised curve, exceeding a criterion, is interpreted as the probability of failure

3 Back-analysis case of an ESS-driven fault slip event

In the previous section, the Triangulation-ESS methodology was proposed to quantify seismic hazard associated with weak geological features in a particular stress field. The potential for shear deformation along structure and lithology contacts, assuming low shear strength, is assessed by ESS and depends on the geology model and in situ stress state assumption. In this section, a more detailed back-analysis is done to simulate the seismic source through boundary element numerical modelling of ride (non-linear shear deformation).

A major effort was spent to import the triangulation as DD elements, improve element shapes and close gaps in the surface. Furthermore, elements defining stope-free surfaces are likely to yield unstable numerical results when they are subparallel and close to other elements. Careful model building was also required to improve elements around such geometries. One conclusion from this work is that this detailed modelling is not feasible for routine implementation of seismic hazard assessment for complex geological models. However, the process was followed here for a smaller area to back-analyse a damaging seismic event and compare modelled versus recorded seismic deformation.

Section 3.1 describes the seismicity around the area, including an event that caused damage which prompted the investigation. The area is in fact as discussed in the previous section and similar picture views are shown. The BIF lithology is then discussed in Section 3.2 where the one contact is known to be weak and conceivably poses a seismic hazard.

3.1 Damaging magnitude 1.8 seismic event

Around the area of interest discussed in the previous section, an MW1.8 seismic event (MW ≡ moment magnitude) occurred on 2 March 2022 at 07:30 causing a significant fall of ground (FOG). Observed support damage included breaking the shotcrete (60 mm) and mesh layers (5.66 mm welded mesh), and causing the failure of two resin bars (3 m) and two split sets (1.2 m). The falling material consisted of rock and shotcrete layer with dimensions of 4.0 × 3.0 × 0.3 m (7,000 kg) and 3.0 × 2.0 × 0.3 m (4,000 kg). No previous damage in the support system was observed. The drive was developed in mafic metavolcanic rocks (meta-andesite [MAN]

– UCS of 104 MPa) in contact with mafic metavolcanic rocks with schistosity (chlorite schist altered meta-andesite [MANX]). The rock mass rating rock quality is between 70 and 80. Seismic response around this area has increased since the beginning of 2022, even though stoping was limited.

Although damage was significant, no location of intense damage was observed where a shear rupture may have 'daylighted' into the excavation. This suggested that the event was more likely associated with a geological structure some distance away and causing the local rock and shotcrete ejection (or shakedown damage).

Seismic system coverage was not good in this area, due to a limited number of sensors in proximity. The closest operational site was approximately 250 m from the damaged area, and the next site 430 m. It can be expected that the location is inaccurate, with the probable location being outside of the coverage area. The magnitude estimate should however have been reasonable for this magnitude event and associated lower-frequency seismic radiation. Seismic moment tensor analysis did not provide a reliable potential source plane orientation, and the location did not indicate a specific structure associated with events. The best estimates of seismic parameters suggest that the event was not directly associated with the damage, in agreement with the damage observation, and that the seismic source was rather some distance away from the drive.

The local conditions in terms of rock lithology and possible stress concentration along the drive could also have played a role, possibly causing the high-energy rock slab ejection.

An MW1.6 seismic event followed two months later, also causing damage, and in general a number of larger events occurred over this time period (14 events MW > 0.0 since the beginning of 2022). Stoping was minimal in this area in terms of volumes and rate, but a significant, unexpected seismic response occurred. Figure 5 is a plan view of the area, showing all recorded events during the four months prior, with symbol colour and size reflecting time and magnitude respectively.

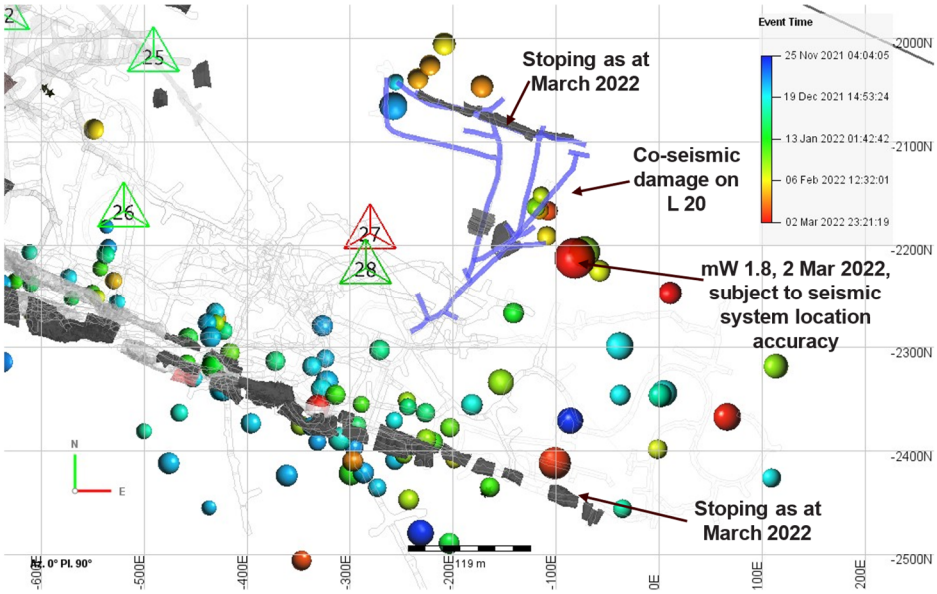

Figure 5 Plan view plot of all seismic events recorded around the mining below level 19, from November 2021 to March 2022. The MW1.8 seismic event that caused damage along the 20 level access drive is indicated. The shaded solid shapes represent the stoping at the time, with the development at the time in proximity to the area of interest also shaded

Mining is relatively deep at approximately 1,000 m, therefore high-stress conditions prevail around excavations, with tunnel squeezing occurring in other parts of the mine. It is important to note that this orebody is located in a deep part of the mine with few excavations around, being an extension to the main orebody. Thus, low induced stress was expected for the FOG location. More-extensive stoping can be seen to the south, with lower seismic response as reflected by the event symbol sizes. The seismic response and

damage were therefore not anticipated, and due to the limited seismic coverage, there was no obvious interpretation of a seismic source.

Understanding the in situ stress distribution is essential for anticipating potential rockbursts or other dynamic failures, which are exacerbated by high stress concentrations caused by mining activities. Therefore, careful monitoring and assessment of the stress environment around the orebody are crucial for the safe and efficient extraction of resources.

3.2 BIF contact as potential seismic source

Geological structures, including lithology contacts, can always be considered potential seismic sources, again subject to their strengths, orientation in the stress field and spatial extent. The BIF contact is a well-known weak structure in this mine, historically also responsible for stope overbreak and other rock mass failure mechanisms. The BIF contact was observed and inspected around the area of interest and was obviously weak and of low shear strength. A photograph is shown in Figure 6. The contact can be described as a graphitic schist and does pose ground control problems in other areas of the mine.

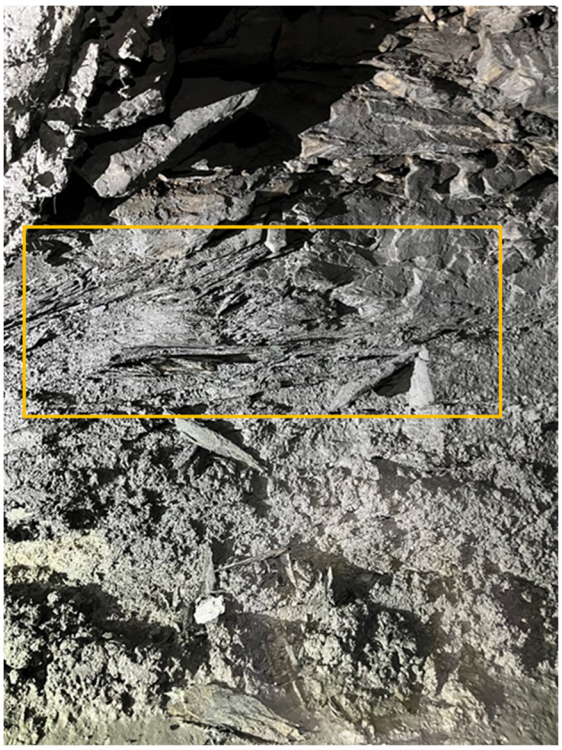

Figure 6 Photograph of the banded iron formation contact in a drive sidewall, showing the laminated graphitic zone, evidently weak in shear

At the area of interest, the graphitic schist is the footwall contact of the BIF lithology, and even though this structure is some distance from the drive damage, it was considered as a likely seismic source due to its evidently weak shear strength.

3.3 Modelled shear slip for structure seismic hazard

A shear slip seismic event can be seen as a rupture initiating at some point, with the rupture front expanding firstly due to shear loading exceeding the internal strength and clamping (referred to as apparent stress in seismic terminology), and secondly momentum of the rock mass. It can be assumed that shear stress exceeding shear strength over large areas, typically tens of metres, along a structure at an approximate constant plane orientation poses a seismic hazard. For an undulating surface, it is unlikely that momentum can be maintained and therefore the rupture front would rather terminate.

The following parameters can be derived from modelling as simulations and quantifications of co-seismic shear slip along a plane of weakness and are proposed to correlate modelled with recorded shear slip events.

3.3.1 Geological structure excess shear stress

This seismic event back-analysis is from the mining area in Section 2, where the complex BIF structure was shown. It will be virtually impossible to model the structure as DD elements. The full structure was simplified by considering the Triangulation-ESS results shown in Figure 3 and focusing on the potential shear slip area on the footwall contact, unclamped by the stoping. This sub-area is shown in Figure 7, which is much smaller than the initial BIF structure, but a considerable effort was still required to set up suitable elements for the model to converge.

The first model step, in Figure 7a, is pre-mining (i.e. the assumed virgin stress state). From the contour colours it can be seen (green to yellow) that the structure at its orientation in the stress field is already in a loading state close to zero ESS, suggesting that any mining-induced unclamping is likely to increase ESS to positive. This is shown in Figure 7b for the model step including the mining up to March 2022, when the event was triggered. The significant impact of mining is seen, in particular the area where the oredrive and stoping are intersected by the structure.

The question remains whether this area of increased ESS and the level thereof is sufficient to generate an MW1.8 seismic event. Although there are some rules of thumb around estimating moment magnitude of events from ESS, it is really required to do non-linear fault slip modelling, and this is discussed in the next section.

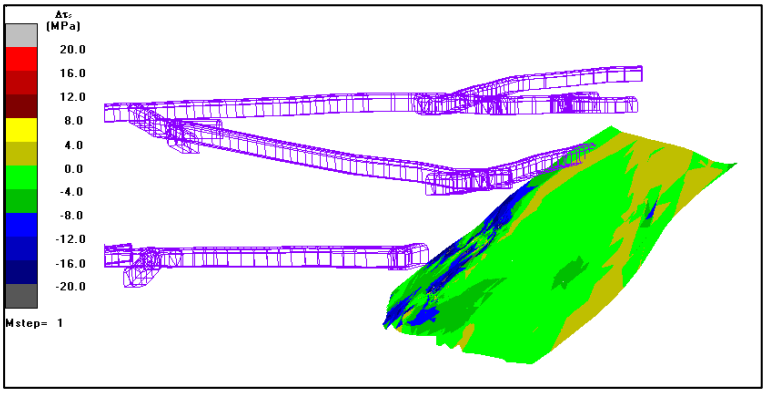

(a)

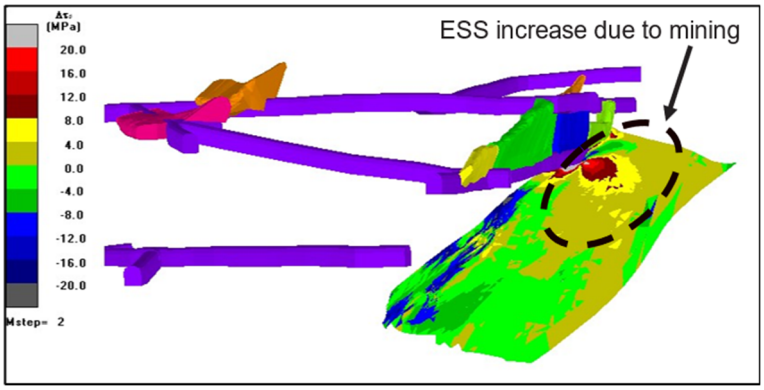

(b)

Figure 7 A sub-area on the banded iron formation footwall structure was selected, guided by the Triangulation-excess shear stress (ESS) results, for which the structure was built as displacement-discontinuity elements for elastic and ride modelling. (a) ESS is shown for the assumed virgin stress state with no mining excavations; (b) ESS is shown for the local drives and stoping as indicated by the solid shapes. For the structure at this orientation in the stress field, the results suggest that a significant increase in ESS is possible

3.3.2 Modelled ride

The elastic boundary element code (*Map3D*) allows modelling of ride for DD elements. Elements under positive ESS can slip in shear and transfer shear stress to neighbouring elements, and this is iterated until all elements are under ESS < 0 MPa, yielding a 'lobe' of ride which can be visualised and quantified.

The so-called 'volume of ride' (Ryder 1988) can be calculated as shear displacement multiplied by area, summed for all elements. It is equivalent to the shear component of the seismic potency tensor (Mendecki & Van Aswegen 2001) considering that the area of modelled ride (shear slip) on a structure is an estimate of a seismic event slip area.

Volume of ride, or modelled seismic potency (P), can be estimated from the modelled ride per boundary DD element as:

$$\mathrm{P} = \sum_{i=0}^{n} a_i \times d_i \qquad (2)$$

where:

a and d = area and shear displacement, respectively, and summing over all elements (weighted sum).

It is therefore a model estimate of the size of a shear slip seismic event.

Modelled ride is shown in Figure 8, which looks different than ESS because of the non-linear deformation process where shear stress is transferred to neighbouring elements, ultimately reaching a final shear deformation stage. The outlined area simulates the co-seismic shear deformation area on the BIF contact, and hence the volume of ride can be quantified according to Equation 2:

- Weighted sum ≡ volume of ride ≡ modelled seismic potency P ~ 21 m^3.

Figure 8 The same view as Figure 7, showing the third model step when the displacement-discontinuity element surface was allowed to yield in shear deformation. The outlined area simulates seismic fault slip area, which can be quantified in terms of modelled seismic potency

This outcome is dependent firstly on the stress state assumption, and secondly on the Mohr–Coulomb shear strength parameters, and therefore subject to model calibration. The stress state in this area is believed to be sub-horizontal, and approximately perpendicular to the BIF structure, at a maximum k-ratio of 1.9.

Furthermore, the assumed cohesion and friction angle is also similar to previous analyses, and in this case, were derived as follow:

- Peak cohesion C = 4 MPa, peak friction angle φ_f = 2°.
- Residual cohesion C = 0 MPa, residual friction angle φ_f = 22°.

3.3.3 Recorded seismic moment

Seismic potency (P) is related to seismic moment (M) as follows (Mendecki & Van Aswegen 2001):

$$M = P \times G \tag{3}$$

where G is rigidity (shear modulus), taken as 33 GPa.

- Recorded seismic moment = 7.473e + 11 Nm.
- Recorded seismic potency = 22.6 m^3.

Moment magnitude can be calculated from seismic moment (M):

- Moment magnitude MW = 0.667 log(M) – 6.1 = 1.8.

This relates to local magnitude but based on source deformation only. In this way recorded seismic event magnitude can be correlated with modelled magnitude in terms of the area and magnitude of co-seismic shear slip.

3.4 Correlation between modelled and recorded seismic event

The previous section stated the modelled volume of ride versus recorded seismic potency. Although good correlation is subject to the shear strength parameters chosen, the values are plausible and the modelled seismic source is convincing. It was discussed in Section 3.1 that good seismic information was unfortunately not attainable due to seismic coverage, therefore the location is not well restrained and the seismic moment tensor solutions could not be derived. However, there was agreement between mine geotechnical engineers and mine seismologists that the BIF weak graphitic schist contact is a potential seismic source, and according to the geology model an area could be found where this structure is likely to slip under the prevailing stress state and mining-induced stress change.

The back-analysis provided a plausible explanation of the seismic event and hence the seismic hazard posed by this structure. Furthermore, confidence is provided in the stress state and structure shear strength assumptions, and these parameters should give realistic estimates of the potential seismic hazard for planned mining.

These modelling assumptions, together with the Triangulation-ESS methodology, are now applied to planned mining as included in the life of mine.

4 Modelled structure seismic hazard for planned mining

4.1 Seismic hazard assessment relative to stoping

The Triangulation-ESS methodology is now applied to the full BIF structure, using the best geology interpretation. In the plan view in Figure 9, the full BIF lithology model is shown, appearing in grey shade but in fact consisting of triangular elements of average area size around 10 m^2. The number of elements is approximately 640,000.

Although ESS results are calculated for the full structure, it is aimed to quantify seismic hazard per mining level as an indication of the trend to be expected for the planned mining sequence. Therefore, structure elements are spatially filtered around the various mining levels, with level 24 shown as example in Figure 9. These points are coloured according to the ESS legend, and this can be inspected in more detail in 3D

geotechnical software, such as GEM4D (Basson 2024), to understand how the BIF structure can pose a seismic hazard to mining on that level.

The statistical procedure described in Section 2.2 can be applied to quantify the level of overstressing, and the expected trend in seismic hazard can be derived per planned mining level. This is given in Figure 10, as a graph of ESS_PoF per mining level. The dotted reference line is the same calculation for mining around historical levels 20 and 21, and therefore serves as a reference for the future expected seismic hazard. This study therefore suggests that seismic hazard will be higher during level 24 mining but then follow a decreasing trend. Visual inspection indicates that this is mainly due to the planned stoping relative to the structure, but in addition, the structure geometry and spatial extent thereof also determine the value of ESS_PoF.

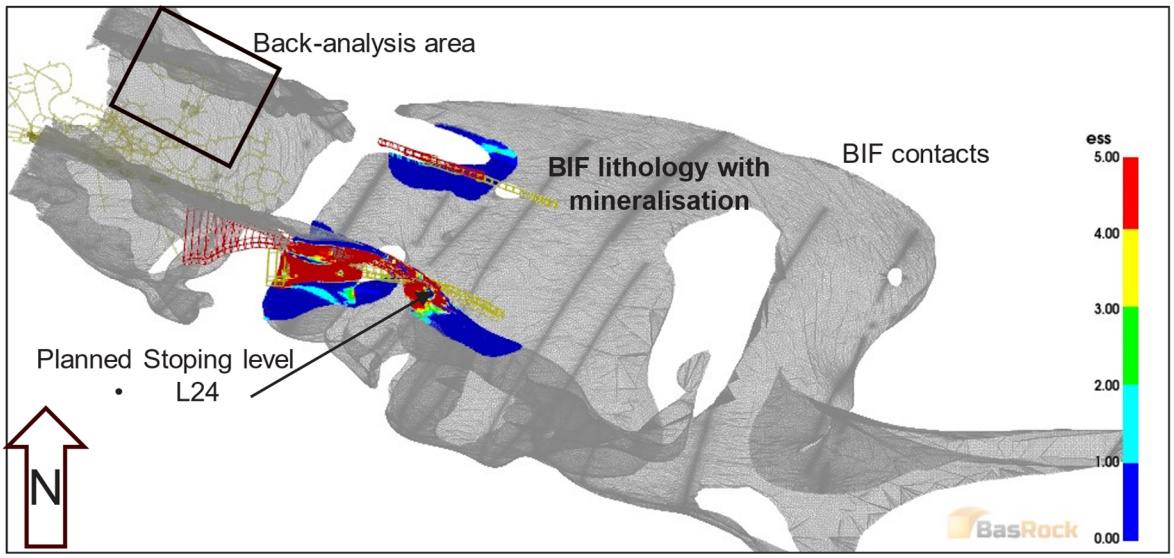

Figure 9 Plan view showing the full banded iron formation lithology geological model down to 2,000 m depth. Although this appears to be a grey shade, the complex geology in fact consists of triangular elements. Excess shear stress results spatially associated with planned level 24 stoping are shown as the colour contours. The back-analysis area of the damaging seismic event can also be seen

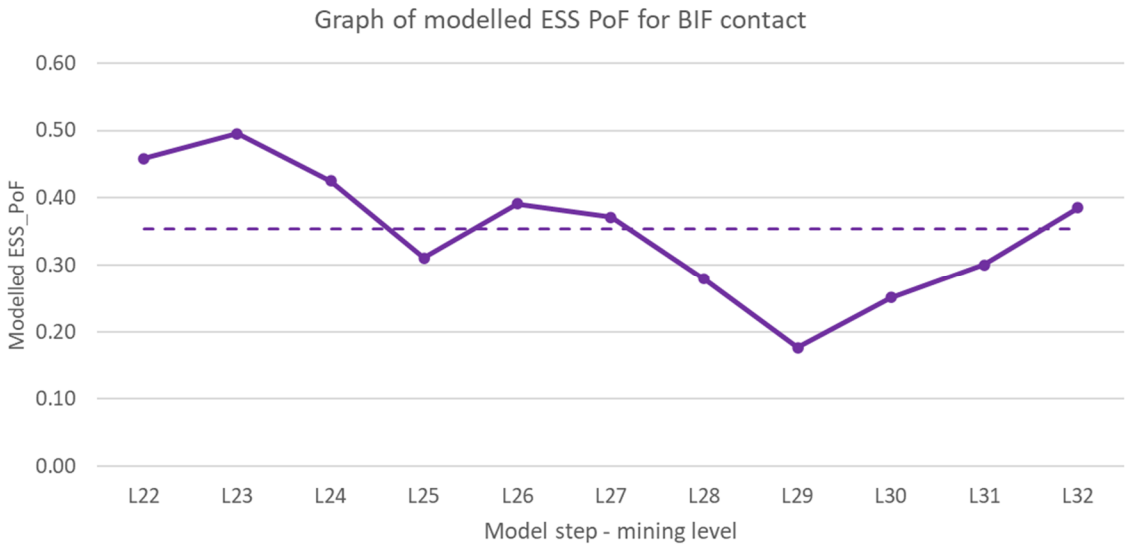

Figure 10 A graph of ESS_PoF, derived according to the proposed statistical method, as an indication of the trend of expected seismic hazard for planned mining. The dotted line reflects the historical mining around levels 20 and 21, therefore serving as a relative indicator of future seismic hazard

4.2 Seismic hazard assessment relative to development

Another application is to quantify seismic hazard associated with development, posed by a geological structure. Access drives can be represented by points spaced at 5 m typically, with these points potentially within a particular distance to a seismically hazardous structure. For this, Triangulation-ESS points are spatially selected within a search radius around an access drive point, and the statistical procedure of Section 2.2 can again be applied to calculate ESS_PoF as the seismic hazard indicator. Therefore, the proximity to, and level of, ESS loading is quantified and can be visualised in 3D.

Figure 11 shows how this is implemented for the back-analysis area of interest. In Figure 11a, one point along the drive is taken as example, and the Triangulation-ESS points are shown within a 150 m radius. From these, ESS_PoF is calculated, which is done for all points along the access drive in Figure 11b, as visualisation of seismic hazard relative to development. In Figure 12, the same is done along the planned development (i.e. the BIF contact Triangulation-ESS points as in Figure 9). Several footwall drives are at such a location relative to the BIF structure that an increase in seismic hazard should be anticipated. From a modelling point of view, this can be addressed by limiting extraction ratio, placement of the drives, and mining sequence to limit exposure to the seismic hazard. Furthermore, the results can be used to guide the implementation and design of dynamic ground support.

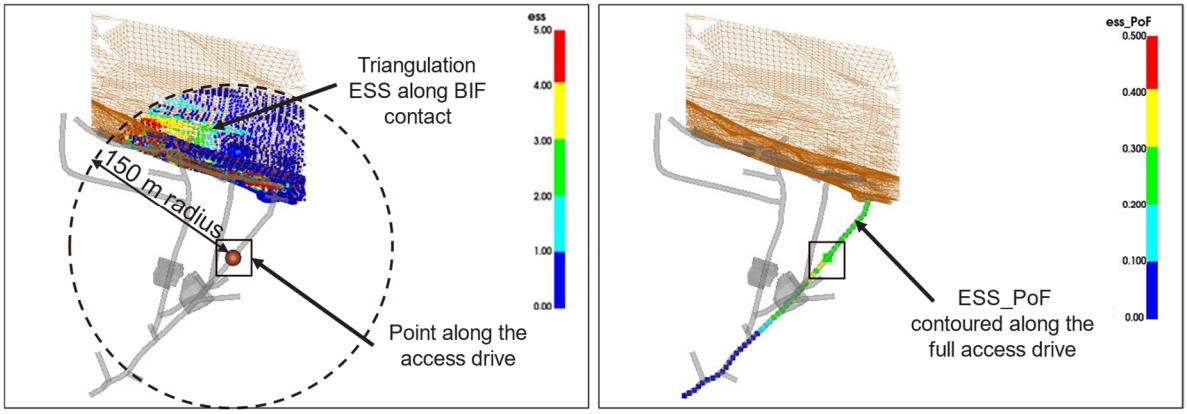

(a) (b)

Figure 11 An example of quantifying seismic hazard relative to development, which is taken from the back-analysis discussed in Section 2. (a) A point along the level 20 access drive is taken, and Triangulation-excess shear stress points of the banded iron formation footwall contact are selected spatially within a 150 m radius. This is done for all points along the drive; (b) ESS_PoF is contoured as an indicator of seismic hazard associated with the geological structure

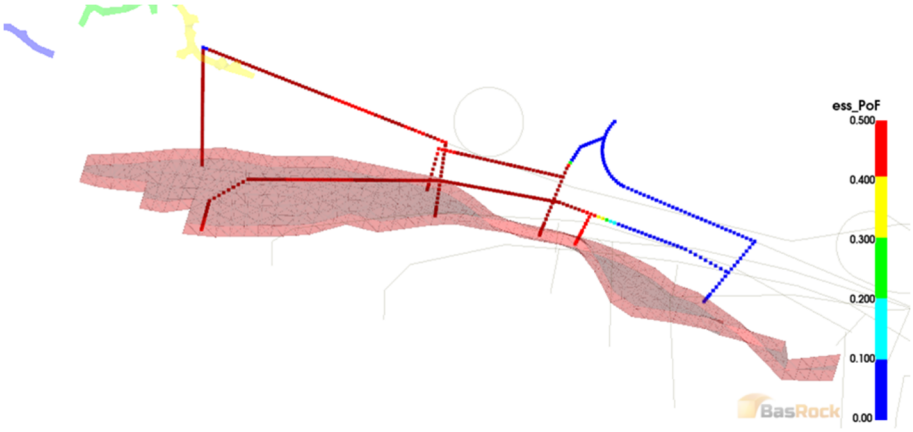

Figure 12 Plan view of the planned level 24 mining, where some access drives are assessed in terms of seismic hazard associated with the banded iron formation structure. The Triangulation-excess shear stress results are not shown, but only ESS_PoF is quantified along the selected drives.

5 Conclusion

A methodology is proposed for use in mine-wide seismic hazard assessment of complex geological structures, including a planned mining layout. A mine geology model can be large, complex, and include multiple structures, and importing all these structures into a boundary element stress model is not feasible for a mine-wide assessment. Geological structure models from a mine site are usually good for visualisation and, for example, identifying intersections of stoping and development with structures, but the triangulation elements can be unsuitable for numerical modelling. In general, non-linear modelling of shear slip will not be feasible, and numerous points that will not contribute to the data interpretation can be discarded.

Subject to the accuracy of the geological model, calibration of structure shear strength properties and the stress state assumption, it should be possible to deduce relevant results regarding structure seismic hazard. Good seismic data and underground observations of seismic damage should allow for the calibration of model properties, and this will improve the efficiency of the methodology. It was shown how the initial elastic assessment guided identification of potential fault slip events associated with structures, which could then be used to do more detailed analysis.

The methodology is based on standard stress tensor transformations, and it was demonstrated that large models can be managed, consisting of literally millions of points defining multiple, complex structures.

A statistical quantification of modelled overstressing is also proposed. This was implemented to assess the long-term seismic hazard of a planned mining sequence down to 10 mining levels deeper, considering the overall stoping layout as well as designed development. The proximity to seismically hazardous structures, and orientation of structure components in the stress field, are the key driving factors.

Acknowledgement

I would like to acknowledge my colleagues who contributed to this work.

References

Basson, F 2024, *GEM4D*, computer software, BasRock, Perth, www.basrock.net

Ford, C 2020, *Research Data Service + Sciences, Understanding Empirical Cumulative Distribution Functions*, University of Virginia, Charlottesville, https://data.library.virginia.edu/understanding-empirical-cumulative-distribution-functions/

Hofmann, G, Scheepers, L & Ogasawara, H 2013, 'Loading conditions of geological faults in deep level tabular mines', *Proceedings of the 6th International Symposium on In-situ Rock Stress*, Sendai.

Mendecki, AJ & Van Aswegen, G 2001, 'Seismic monitoring in mines: selected terms and definitions', in G Van Aswegen, RJ Durrheim & WD Ortlepp (eds), *Proceedings of the Fifth International Symposium on Rockburst and Seismicity in Mines*, South African Institute of Mining and Metallurgy, Johannesburg.

Python 2024, *Python*, version 3.11.2, https://www.python.org

Ryder, JA 1988, 'Excess shear stress in the assessment of geologically hazardous situations', *Journal of the South Africa Institute of Mining and Metallurgy*, vol. 88, no. 1.

Wiles, T 2024, *Map3D*, computer software, version 68, Map3D International Ltd, www.map3d.com